Thin Solid Films 791 (2024) 140239

Contents lists available at ScienceDirect

Thin Solid Films

journal homepage: www.elsevier.com/locate/tsf

High throughput physical vapor deposition growth of $Pb(Zr_xTi_{1-x})O_3$ perovskite thin films growth on silicon substrates.

Ioanna Bakaimi [a,*], Brian E. Hayden [a], Colin J. Mitchell [b], Goran Z. Mashanovich [b]

[a] School of Chemistry, University of Southampton, Southampton SO17 1BJ, UK
[b] Optoelectronics Research Center, University of Southampton, Southampton SO17 1BJ, UK

A R T I C L E I N F O

Keywords:
Lead zirconate titanate
Thin films
Physical vapour deposition
Perovskites
High throughput synthesis
Combinatorial screening
Silicon photonics

A B S T R A C T

The integration of lead zirconate titanate ($Pb(Zr_xTi_{1-x})O_3$) (PZT) compounds on Si substrates with a smooth surface would provide a key technology for silicon photonic devices. The quality of the deposited thin film is critical in order to integrate $Pb(Zr_xTi_{1-x})O_3$ on Si substrates for applications such as pyroelectric mid-infrared detectors or optical modulators. Here, we have applied physical vapour deposition technique using a modified molecular beam epitaxy tool to deposit perovskite $Pb(Zr_xTi_{1-x})O_3$ on Si and Pt substrates. We have developed a method to grow crack-free PZT films on Si substrates. The fabrication procedure entailed the use of TiO_2 as a buffer layer and post annealing of the PZT/TiO_2/Si films under oxygen atmosphere. Cross section Scanning Electron Microscopy images enabled the identification of two distinct layers: PZT and TiO_2, which was also confirmed by Spectroscopic Ellipsometry. X-Ray Diffraction patterns indicated the transition from the rhombohedral to the tetragonal phase and the formation of the perovskite phase of $Pb(Zr_{0.44}Ti_{0.56})O_3$.

1. Introduction

Lead zirconate titanate $Pb(Zr_xTi_{1-x})O_3$ thin films, usually referred to as PZT, are widely known for their excellent optical properties and their outstanding dielectric behaviour at room temperature [1,2]. The former can be evidenced for example by high refractive index and large electro-optical response measured by the Pockels effect [3] whereas the latter is observed by the superior pyroelectric, [4] piezoelectric and ferroelectric properties [5] at room temperature. Therefore, there is a plethora of optoelectronic and dielectric applications, which would greatly benefit from the integration of PZT thin films on Si based substrates [6–10]. Examples of such applications include: low power silicon photonic phase shifters/modulators [11] used in data centres and Light Detection and Ranging (LiDARs). Additionally, motion sensors, smoldering fire detectors, uncooled thermal imagers, radiometer and gas/-laser analyzers all include a room temperature pyroelelectric element, such as PZT [12].

Although PZT thin films have been widely studied, the realization of their full potential as possible materials for integration in silicon photonic devices is hindered by two factors. First, most studies focus on PZT compounds that are integrated on non-Si substrates such as Pt [13–15], sapphire [16], ZnO [3] and Nb [17]. These reports entail growth of thin films by Radio Frequency sputtering [18,19], acetate solution [20], sol gel [10,21–23], Metal Organic Chemical Vapor Deposition [24], or pulsed laser deposition [7]. Second and most important, cracks, hillocks and whiskers have also been reported as major problems in PZT thin films after its sintering, not only on Si but even on Pt substrates [25]. On Si substrates, the direct deposition of PZT thin films has proved challenging due to the diffusion of lead into Si and subsequently the formation of silicides which led to cracks and whiskers on the films surface.

Much experimental work has been focused on improving the surface morphology of PZT thin films on Si substrates. Most of the relevant reports utilize a buffer layer such as Ti or Zr [18], Zn [26,27], $La_{0.5}Sr_{0.5}CoO_3$ [28], Pt [29], $SrTiO_3$ [30], ZrO [31], MgO [32], Ni-Al [33] and thin lanthanide layers [34]. The choice of appropriate buffer layers should result in a crack-free and smooth PZT surface. Another important consideration is that its growth should be technologically simple and cost effective, which would facilitate the fabrication of PZT on Si substrates in devices on a mass manufacturing scale.

Depending on the device that PZT will be integrated with, different PZT ratios of Zr/Ti are favourable. For example, it is known that the optoelectronic devices that exhibit optimum Pockels effect are characterized by the tetragonal structure with oriented growth along the a-axis [35,36]. Whilst the optical and Electro-Optical (EO) response of PZT

* Corresponding author.
E-mail address: i.bakaimi@soton.ac.uk (I. Bakaimi).

https://doi.org/10.1016/j.tsf.2024.140239
Received 21 April 2023; Received in revised form 28 December 2023; Accepted 25 January 2024
Available online 26 January 2024
0040-6090/© 2024 The Authors. Published by Elsevier B.V. This is an open access article under the CC BY license (http://creativecommons.org/licenses/by/4.0/).

thin films grown using various methods has been reported with an emphasis on optimisation through orientational growth, less attention has been paid to the details of composition and dopants, which can strongly influence the optical properties. This is evidenced by the fact that the majority of the published results are related to a limited number of Zr/Ti ratios, mainly focusing on the $Pb(Zr_{52}Ti_{48})O_3$ [37] or the $Pb(Zr_{30}Ti_{70})O_3$ [38] compositions.

Direct growth of PZT phase has been reported on Pt coated substrates (a $Pt/Ti/SiO_2/Si$ structure referred to as 'SSTOP') using High Throughput Physical Vapour Deposition (HT-PVD)[13,14]. HT-PVD allows the formation of a wide range of compositions on the same film with the use of wedge shutters that are placed above the flux of the evaporated material [39,40]. The HT-PVD method that we have applied [39] has been used for the formation of various materials and products such as fuel cells [41], tunable dielectrics [42] and materials for solid states batteries [40]. These studies[13,14] have achieved the perovskite PZT phase by depositing PZT at room temperature and then post annealing in a tube furnace at 700 °C [13] to achieve optimum crystallinity of the PZT phase.

Here, we report the growth of PZT on SSTOP substrates, hereafter referred to as 'Pt' as well as on Si substrates, using the same HT-PVD method, utilizing combinatorial synthesis and screening. It is important to highlight that PZT film growth on platinized substrate is widely used in the industry for example in piezoelectric actuators, ferroelectric memories, capacitors or pyroelectric detectors. The present research indicates the possibility to grow PZT on Si without Pt or any other bottom electrode layer. We have achieved growth of PZT thin films on Pt substrates by room temperature deposition and post annealing at 620 °C under continuous oxygen atmosphere. Additionally, we have eliminated the formation of cracks and whiskers with the use of TiO_2 buffer layer on top of the Si substrate. This way we have developed compositional libraries of PZT thin films materials on individual Si chips. The stack of PZT on TiO_2/Si was confirmed by Scanning Electron Microscopy (SEM) measurements. X-Ray diffraction (XRD) and Raman spectroscopy confirmed the formation of the tetragonal perovskite phase whereas spectroscopic ellipsometry showed that the optical properties of the PZT/TiO_2/Si presented the expected behaviour.

The deposited PZT thin films have a wide range of Zr:Ti ratios which cover both the tetragonal and the rhombohedral phase as confirmed by the XRD patterns, as well as the morphotropic phase boundary. We have applied this method for the growth of PZT thin films with the aim to expand it in the combinatorial development of waveguides and photonic devices which will allow the correlation of fundamental properties such as composition and crystallinity with the overall performance of the device.

2. Experimental procedure

2.1. High throughput physical vapour deposition of PZT thin films

PZT thin films have been deposited at room temperature on SSTOP ('Pt' substrates), on Si substrates with HT-PVD using a modified Molecular Beam Epitaxy (MBE) system from DCA Instruments. The Pt ($Pt/TiO_2/SiO_2/Si$) and Si (orientation ⟨100⟩, P-type boron doped) were purchased from Nova Electronic Materials. There was no SiO_2 on the top of Si, only photoresist which has been removed prior to deposition. Lead slugs (Goodfellow 99.999 %) in Al_2O_3 crucibles were evaporated by Knudsen cells at temperatures ranging between 720 and 747 °C. Zr (Alfa Aesar 99.5 %) and Ti slugs (Alfa Aesar 99.98%) were placed on graphite crucibles and were evaporated using 40 cc electron guns from Telemark. An RF atom source (Oxford Applied Research) provided atoms of oxygen by applying 375 W of RF power, under 1.5 ml min^{-1} of oxygen flow rate. In order to achieve compositional spread, wedge shutters have been placed above the beam of the evaporated materials. The substrates used were 35×35 mm^2 resulting in a deposited area of 29×29 mm^2. The average thickness of PZT thin films was 400–460 nm for 60 min deposition. The deposition was carried out at room temperature so both layers of TiO_2 and PZT were amorphous. To obtain the PZT perovskite phase the PZT/TiO_2/Si stacks were annealed in a tube furnace under oxygen flow at 620 °C for 5 h with a heating rate of 0.4 C/min. During the annealing a 2 % loss of Pb has been measured with the use of high throughput EDX.

2.2. PZT thin films characterization

The elemental analysis of the fabricated films was carried out using SEM and Energy Dispersive X-Ray Spectroscopy (EDXS) using a Tesca Vega 3 equipped with an EDXS detector XMax 50 from Oxford Instruments. The calculation error of the atomic percentage of each element on the EDXS mappings presented in the ternary plots is 2 %. The quantification of the EDXS spectra has been carried out using the software Inca from Oxford Instruments, and the automated option for EDXS mapping. High magnification images were obtained using a ZEISS Sigma Series SEM. The crystal structure was investigated by XRD patterns using a Bruker D8 diffractometer equipped with an Incoatec microsource Cu Kα and a GADDS detector and a vertical Theta/Theta geometry. Raman spectroscopy was carried out using a Horiba XPlora Plus equipped with 532 nm (green) laser, that uses 10 X, 50 X, and 100 X objectives. The spectra presented in this work were obtained with the use of 50 X objective which results in a 0.87 μm diameter laser spot. Layer thickness characterization was further established by the measurement of psi and delta parameters of the PZT films. The method utilized for obtaining these data was spectroscopic ellipsometry (SE) using a J. A. Woollam M-2000 XI Spectroscopic Ellipsometer. The data were subsequently analysed using J. A. Woollam's CompleteEASE software to provide thickness data. Additional thickness measurements were carried out with a Bruker DektakXT stylus surface profiler.

3. Results and discussion

3.1. Composition ternary plots

Fig. 1 shows the ternary plots of the compositional spread from some representative PZT thin films that have been deposited for this work and calculated by EDXS mapping. The shaded area corresponds to ±10 % spread along the pseudobinary line of 50 %/50 % for Pb/Zr.

We have fabricated thin films in the compositional area around the transition (blue line) from rhombohedral (RH) to tetragonal (T) and

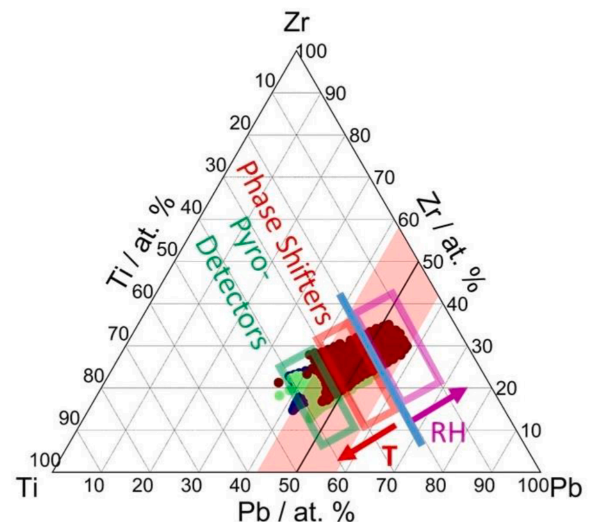

Fig. 1. Compositional spread of $Pb(Zr_xTi_{1-x})O_3$ /TiO_2/Si thin films. The two areas of interest are marked with the red and green rectangles, for optical phase shifters and pyroelectric detectors, respectively.

focus at the tetragonal crystal structure in order to investigate the enhancement of the Pockels tensors, which is marked with the red rectangle in Fig. 1.

Fig. 1 shows the EDXS high throughput mapping as obtained from three different samples which are shown with the red, green and dark blue data points. For each sample we have carried out a 14×14 mapping resulting in 196 data points across the surface of the film. As it can be observed there is a shift from the red to blue data points from the low to rich Ti concentrations. One can notice for example that the red data points spread from low to higher Ti concentrations corresponding to both the rhombohedral and the tetragonal phase. There is an overlap of these: the blue, red and green points, as these three samples have common composition spread around the center of the ternary plot. In order to achieve optimum results for pyroelectric detectors the Ti percentage should be above 35 %, which is the area marked with the green rectangle in Fig. 1. The EDXSmeasurements results in the calculation of the atomic percentage of each element and takes into account that the sum of the three elements is: (Pb+Zr+Ti) =100 % where the (Zr+Ti)= 50 %.To retain the perovskite stoichiometry (ABO_3) the Pb percentage was maintained around 50 % (± 7 %) and the sum of (Zr+Ti) was also around 50 %(± 7 %). We aimed for a small excess of Pb during the deposition (+5 %) to compensate for a possible loss of Pb during the post annealing treatment.

3.2. Thin films fabrication of PZT on Pt and si substrates

Initially the crystallization of PZT thin films was attempted inside the ultra high vacuum chamber by depositing PZT layers directly on Pt and Si substrates at temperatures ranging from 550 to 670 °C. Although both PZT on Si and Pt were crack free, the perovskite phase could not be identified by the X-Ray graphs.

Then, room temperature PZT deposition in the vacuum chamber was carried out on Pt and Si substrates followed by post annealing in a tube furnace. In detail, PZT was deposited directly on SSTOP and Si substrates at an oxygen partial pressure of 1.86×10^{-4} Pa. Subsequently, the films were annealed at 620 °C for 5 h, in a tube furnace under oxygen flow. After cooling at room temperature XRD measurements indicated the formation of the tetragonal perovskite phase. Fig. 2 shows the formation of the PZT tetragonal phase on Pt substrates (upper graph) and on Si (bottom graph) indexed upon the ICDD databased PDF card 00–050–0346. It is worth mentioning that the perovskite phase was stable at room temperature both on Pt and Si substrates and even when checking the XRD patterns after 12 months since the perovskite was formed with post annealing. One tiny peak at the bottom of Fig. 2, which is not indexed at 30.5 °C could indicate the possible existence of

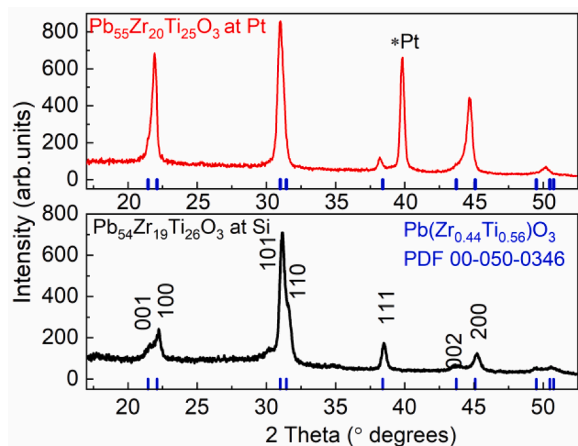

Fig. 2. X-Ray diffractograms from PZT thin films deposited directly at Pt (SSTOP) substrate shown on the top graph and Si substrates (bottom graph) after annealing at 620 °C.

pyrochlore phase, which could only be confirmed with other methods such as High Resolution Transmission Electron Microscopy (HR-TEM). These findings indicate that PZT can be deposited directly on Si and Pt coated substates. Although there were no cracks in the Pt coated films, the main issue is the formation of cracks at the surface of PZT thin films on Si.

The PZT thin films in this study, grown directly on Pt substrates were crack free as it can be seen in Fig. 3. Fig. 3(a) shows grains on the surface of the PZT/Pt thin films which are in agreement with previous findings of PZT thin films [43,44]. The surface morphology shows grains of rosette-type morphology (Fig. 3(b)) which have been found also in other reports that indicate the possible formation of theperovskite structure [45]. According to other reports[46], the dimensions of the Pt grains mainly control the PZT grain diameter, so the grain morphology in PZT perovskite thin films is not standard.

3.3. SEM studies of PZT/TiO_2/Si thin films

The use of a TiO_2 buffer layer was necessary in order to develop PZT on Si thin films without cracks and whiskers. First, the TiO_2 was deposited at room temperature in the vacuum chamber and subsequently the PZT layer was grown at an oxygen partial pressure around1.06×10^{-4} Pa. The stack of PZT/TiO_2/Si was then annealed at 620 °C for 5 h, with a rate of 0.4 °C/min under continuous oxygen flow. The perovskite phase of the PZT formed after the annealing was stable at room temperature.

Although the perovskite phase was formed after annealing, the PZT thin films deposited on both Si and SiO_2 demonstrated severe cracks and various whiskers at their surface. Fig. 4(a) shows a PZT/Si thin film after annealing with a high density of cracks with even distribution along the films surface. There is a ‘tile’ like morphology similar to that observed for Nb, Sb and Mn doped PZT thin films prepared with the sol gel technique [47]. PZT thin films prepared with RF sputtering after annealing [48] also showed cracks but these were smaller and thus denser (around 20 μm). The cracks presented in Fig. 4(a) are quite large, with sizes ranging from 100 to 300 μm.

In order to prevent the cracks and silicides on the surface of the PZT thin film, buffer layers of TiO_2 have been deposited at room temperature prior to depositing the PZT thin film. Initially thinner layers (TiO_2 thickness <200 nm) have been investigated. However, whiskers have been observed at the surface of those samples. The surface of a thin film with a TiO_2 buffer layer of 170 nm is shown in Fig. 4(b).

After further experimentation, it was found that a 250 nm TiO_2 buffer layer was sufficient to stop the cracks and silicides forming after annealing. A crack free surface of a PZT/TiO_2/Si thin film is shown in Fig. 4(c). A cross section image of PZT/TiO_2/Si (the upper part of Fig. 5) shows two distinct layers above the Si layer: the TiO_2 buffer layer and the deposited PZT.

A higher magnification image of PZT/TiO_2/Si (scale bar 400 nm at the lower part of Fig. 5) confirms that there are no cracks, silicides or pin holes at the surface of the PZT layer. The high magnification image shown in the lower part of Fig. 5 not only confirms the absence of cracks but also might indicate the possibility of having the perovskite phase as shown with the rosette grain and a secondary phase, possibly the pyrochlore [49], which surrounds the perovskite phase. As it will be discussed later, no secondary phase was detected with XRD for the PZT/TiO_2/Si films.

The thickness of these layers as estimated by the SEM were around 425 nm for the PZT layer and 258 nm for the TiO_2 layer. Single point EDX analysis was carried out in some points on each of the layers while doing the cross section SEM measurements. We have measured a small atomic percentage(≤10%) of Pb in the TiO_2 layer and most importantly no Pb was detected in the Si substrate, verifying that the TiO_2 film acts as a barrier layer for the diffusion of Pb into the Si.

As the motivation of this work is to fabricate PZT devices, it is worth mentioning here that the use of a 250 nm thick TiO_2 layer in the PZT

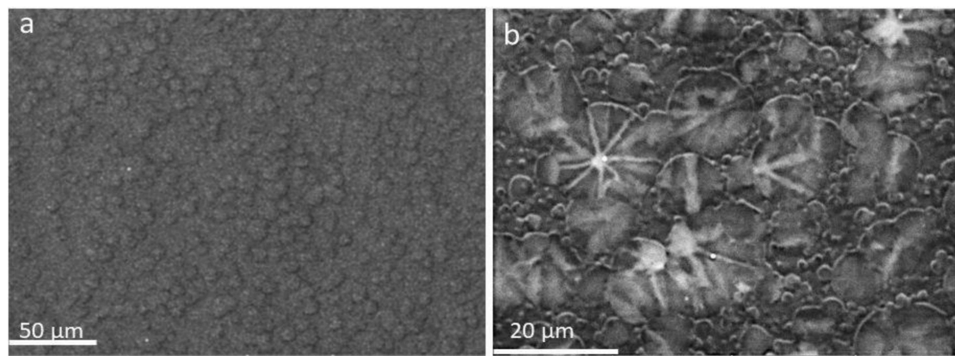

Fig. 3. SEM images from a PZT thin film grown on Pt (SSTOP) substrate.

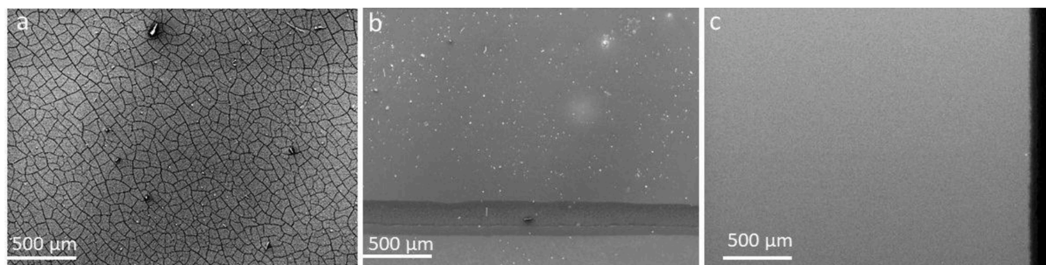

Fig. 4. PZT thin films after annealing at 620 °C: a) PZT/Si without TiO_2 buffer layer b) PZT/TiO_2/Si with a 170 nm thick TiO_2 layer and c) PZT/TiO_2/Si with a 250 nm thick TiO_2 layer.

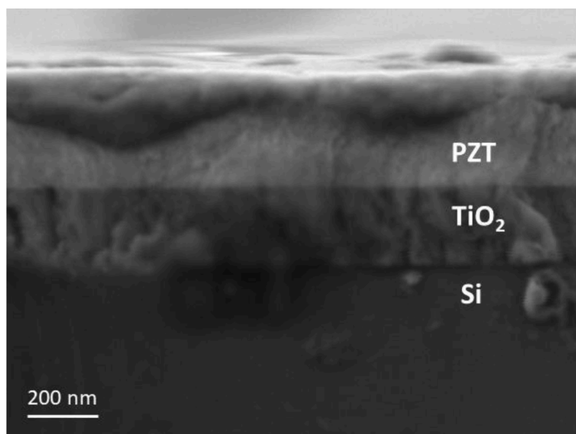

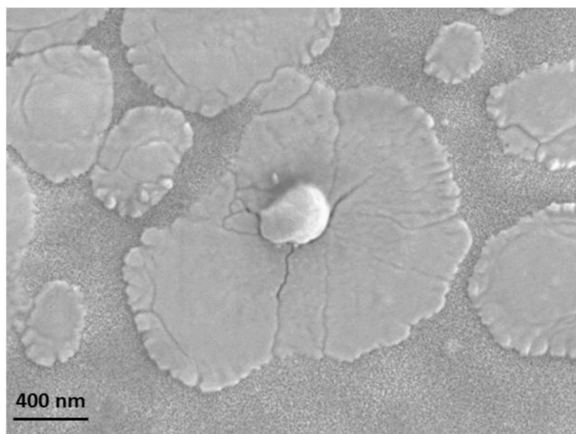

Fig. 5. Cross section SEM image of a $Pb(Zr_xTi_{1-x})O_3/TiO_2/Si$ thin film. Bottom: High magnification SEM image of a $Pb(Zr_xTi_{1-x})O_3/TiO_2/Si$ thin film.

applications will not influence the electro-optic or piezoelectric measurements. The measurement option that will be followed is the deposition of SiN on top of PZT to form a waveguide and then two electrodes on each side to form a field and therefore measure optical properties such as the Pockel's effect, as it has been previously demonstrated by the authors for similar measurements on BTO thin films [50].

3.4. Spectroscopic ellipsometry

Non-destructive Spectroscopic Ellipsometry measurements were carried out on a PZT/TiO_2/Si thin film. A correlation between the Zr/Ti ratio and the refractive index is beyond the scope of this research, so a PZT film with narrow composition spread and the approximate ratio of Zr/Ti= 1/1 was selected for the SE measurements.

Multiple points were analysed across each sample, and at three angles (65°, 70°, and 75°) in order to achieve greater accuracy when fitting simulated material data to the experimental data. Initially, a model for TiO_2 was generated by analysing data from a deposited sample with a single TiO_2 layer on silicon. A Cody-Lorentz band gap oscillator material model was used, and iteratively fitted to the experimental data, when generating plots across a wavelength range (roughly covering 190 to 1700 nm). In this way, values for layer thickness were calculated. Confidence in the fit-point was achieved by contrasting the resulting thickness measurement to probe step-height measurements. Furthermore, SEM images confirmed the approximate thicknesses were correct. Ellipsometry thickness measurements were then carried out directly across the PZT sample to give thicknessesof both the TiO_2 and PZT layers.

The purpose of these measurements was mainly to provide congruent data at a known point demonstrating the existence of two distinct layers, and to extrapolate that across the sample surface non-destructively in order to measure thickness variations and extract the refractive index. The SE thickness analysis verified the SEM measurements confirming average thicknesses of: 230–257 nm for the TiO_2 and 412–464 nm for the PZT layer.

The extracted values of the refractive index n and k for the

experimental data at the angle of 65 ° at wavelenghts between 400 and 1600 nm are shown in Fig. 6. There are numerous reports for the value of refractive index of the PZT material, which ranges between 2.4 and 3.0 depending on the Zr/Ti ratio where higher values of *n* indicate higher Ti percentage [1,51]. The value of *n* can vary with the crystallinity [52] and the form of the material such as ceramic [51] or thin film stacks [53]. The values of *n* shown in Fig. 6 are: 2.82, 2.58 and 2.49 for the wavelengths of 400 nm, 601 and 1000 nm, respectively. Similar values of *n* have been reported [54] for polycrystalline perovskite PZT thin films [52] indicating that the optical properties of the PZT/TiO_2/Si thin films are comparable with other PZT thin films fabricated with other methods.

3.5. X-Ray diffraction

It is very interesting to show how the TiO_2 layer affects the crystallization of the PZT layer and furthermore how the Zr/Ti ratio affects the evolution of the XRD peaks. Fig. 7 shows X-Ray diffractograms obtained from a PZT thin film with a 250 nm TiO_2 buffer layer and various Zr/Ti ratios. The bottom part of Fig. 7 shows two diffractograms with low Ti percentage: the $Pb_{57}Zr_{28}Ti_{15}$ shown with the black colour and the $Pb_{55}Zr_{26}Ti_{19}$ with dark cyan. In both diffractograms the Bragg reflections are indexed upon the rhombohedral space group: R3c (161) of the PDF card 01–073–6947 shown with the magenta vertical tick marks. The X-Ray diffractogram (lower Ti content) shows a shift of the XRD peaks towards the left in respect with the theoretical Bragg reflections position, indicating probably slightly larger cell parameters than the expected ones. As the Ti% atomic content increases the peaks shift towards higher angles, indicating a better agreement with the theoretical cell parameters. During the annealing, the TiO_2 buffer layer crystallizes as indicated by the weak peak at 25° shown with the asterisk in the bottom graph.

The upper part of Fig. 7 shows the transition from the rhombohedral to the tetragonal phase. X-Ray diffractograms with Ti composition of 26–34 % are presented. A broadening of the peaks in respect with the low Ti percentage graphs can be observed. Furthermore, two distinct pairs of peaks emerge: at 21–22° and 30–31° shown in the green plot, which corresponds to a 29 % Ti atomic percentage of a PZT thin films' composition. This probably indicates the transition from the rhombohedral to the tetragonal structure, as these peaks are indexed upon the tetragonal space group P4mm (99) of the PDF card 00–050–0346 shown with the red vertical tick marks. The P4mm space group is non-centrosymmetric allowing properties such as pyroelectricity, piezoelectricity and ferroelectricity. It is worth mentioning that we have examined the GADDS frames of the presented graphs and there was no indication of possible preferred orientation. Earlier reports [55,56] refer to PZT thin films on Pt /Ti/SiO_2/Si wafers with a TiO_2 seeding layer grown with the sol gel method that were characterized by a highly preferred orientation along the [111] axis. C-axis orientation has been observed for PZT thin films grown on Si substrates with a MgO buffer layer [21]. Nonetheless, the indications of a possible secondary phase in the high SEM image (bottom part of Fig. 5), similarly with previous studies [49],as well as the complexity of the thin films' X-Ray diffractograms imposed by various factors (e.g. stress, strain, possible orientation, quality of crystallinity) indicates the necessity to investigate and interpret these data sets across the morphotropic phase boundary with other methods such as High Resolution Transmission Electron Microscopy (HR-TEM) which is beyond the scope of this work.

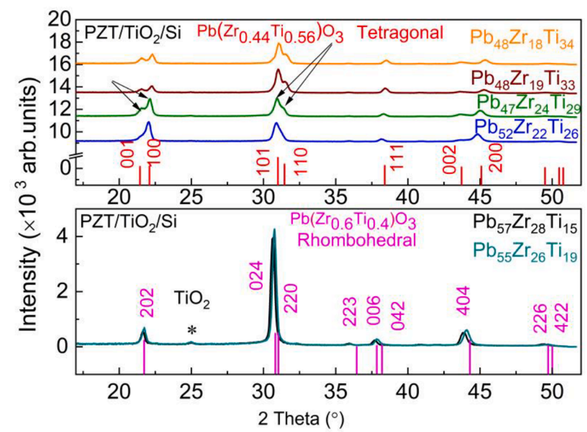

Fig. 7. X-Ray diffractograms of: Bottom graph: PZT/TiO_2/Si with low Ti percentage indexed upon the rombohedral space group whose theoretical Bragg peaks are shown with the magenta vertical tick marks. Top graph: Various graphs from PZT/TiO_2/Si with different Ti percentage indexed upon the tetragonal space group shown with the red vertical tick marks.

3.6. Raman spectroscopy

Raman spectroscopy has been utilized to further investigate the structure of the PZT thin films. Fig. 8(a) shows the Raman spectra of PZT thin films on Pt and PZT/TiO_2/Si is presented in Fig. 8(b). To identify which modes are attributed to the TiO_2 buffer layer and the Si substrate, the Raman spectra of a TiO_2/Si thin film has been measured as well as a substrate of Si, presented in 8(c). Both TiO_2/Si and Si were annealed under identical conditions with the PZT/Pt and PZT/Ti O_2/Si prior to obtain any Raman spectra. All Raman spectra in Figure 8 have been measured under the same conditions. The mode description taken into account is congruent with earlier reports [57,58] for perovskite PZT

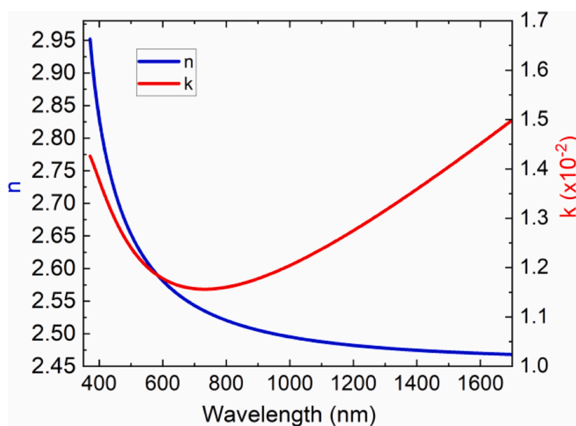

Fig. 6. Extracted complex refractive index for PZT material from SE data. The measurement corresponds to the 65 ° angle scan.

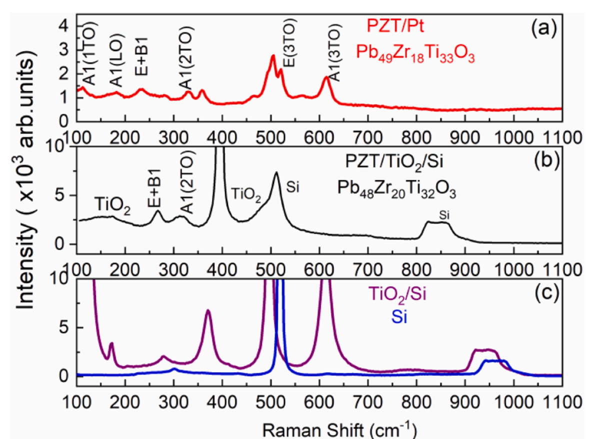

Fig. 8. Raman spectroscopy of: (a) PZT thin films on Pt substrates, (b) PZT/TiO_2/Si, and (c) TiO_2/ Si and Si.

structures. Various Raman modes are recognized [59–61] in the PZT/Pt thin film: A_1(TO) mode at 140 cm^{-1}, A_1(LO) at 183 cm^{-1}, E + B1 at 235 cm^{-1}, A_1(2TO) at 330–355 cm^{-1}, E_3(TO) at 500–520 cm^{-1} and A_1(3TO) at 613 cm^{-1}.

The spectrum of the PZT/TiO_2/Si thin film shows vibrational modes, the majority of which correspond to either the TiO_2 layer or the Si substrate. Specifically, the sharp peak at 520 cm^{-1} and the broad hump between 800 and 900 $cm^{-1}$of the PZT/TiO_2/Si sample with the shift towards lower wavelength, are attributed to the Si layer. The intense peak around 400 cm^{-1} probably originates from the TiO_2 buffer layer. The broad peaks around 250 cm^{-1} and 300 cm^{-1} likely originate from the E + B1 and A_1(2TO) modes respectively, of the PZT structure. The difference in the Raman spectra between the PZT/Pt and PZT/TiO_2/Si is probably due to internal stresses caused by the different substrates [62–64] or the difference in the crystallinity [65].

4. Conclusion

The approach introduced in this work is the use of high throughput physical vapour deposition for the deposition of PZT on Si substrates. PZT films have been grown using combinatorial growing and screening methods in order to investigate the integration of crack free PZT thin films with Si platforms for potential future use in optical modulators and detectors. Two substrates have been used: Pt coated (SSTOP) and Si. The Pt substrates were used for comparison and to aid in some characterization methods as the perovskite PZT has been grown directly on Pt coated substrates using post annealing in order to achieve crystallization and the formation of the perovskite phase. The use of TiO_2 buffer layer was necessary to obtain a smooth and crack free PZT thin film surfaces when depositing on Si substrates. The SEM analysis confirmed both crack free surfaces of the PZT films and cross section SEM images verified the existence of two distinct layers namely the PZT and TiO_2 in the PZT/TiO_2/Si stacks. The use of TiO_2 prevented the diffusion of Pb into Si, and no traces of Pb were detected by EDXS spectroscopy on the Si substrate. The formation of the PZT phase has been confirmed by X-Ray and Raman measurements. The development of PZT-Si based waveguides is the next step of this work as well as a detailed dielectric characterization. The growth method that is presented offers a cost and time effective method for possible integration of PZT crack free films with Si-based material platforms which will utilize the combinatorial synthetic methodology in order to develop high throughput growth of devices. Although there are still significant challenges to be addressed which are related to a complete structural characterization by HRTEM and furthermore, measuring the films' opto-electronic properties such as the Pockel's effect and their piezoelectric response in the future, this work shows that PZT films can be deposited in Si by high throughout physical vapor deposition without the use of Pt bottom (electrode) layer.

Credit authorship contribution statement

Ioanna Bakaimi: deposition of thin films, high throughput screening, measurements and analysis of XRD, SEM, EDX, Raman data,writing original draft and editing of the manuscript. Colin Mitchel: SE and Stylus Profiler measurements and relevant data analysis. Brian E. Hayden and Goran Mashanovich: conceptualization, supervision and providing funding.

CRediT authorship contribution statement

Ioanna Bakaimi: . **Brian E. Hayden:** Conceptualization, Funding acquisition, Resources, Supervision, Validation. **Colin J. Mitchell:** Data curation, Formal analysis, Writing – review & editing. **Goran Z. Mashanovich:** Conceptualization, Resources, Supervision, Writing – review & editing.

Declaration of competing interest

The authors declare that they have no known competing financial interests or personal relationships that could have appeared to influence the work reported in this paper.

Data availability

Data will be made available on request.

Acknowledgment

The EPSRC Grants that have in part funded this research: EP/N00762X/1: 'National Hub in High Value Photonic Manufacturing' and EP/R003076/1 'Rockley Photonics and the University of Southampton: A Prosperity Partnership'

References

[1] N. Izyumskaya, Y.I. Alivov, S.J. Cho, H. Morkoç, H. Lee, Y.S. Kang, Processing, structure, properties, and applications of PZT thin films, Crit. Rev. Solid State Mater. Sci. 32 (2007) 111–202.
[2] J.P. George, P.F. Smet, J. Botterman, V. Bliznuk, W. Woestenborghs, D. Van Thourhout, K. Neyts, J. Beeckman, Lanthanide-Assisted deposition of strongly electro-optic PZT thin films on silicon: toward integrated active nanophotonic devices, ACS Appl. Mater. Interfaces 7 (2015) 13350–13359.
[3] K. Alexander, J.P. George, J. Verbist, K. Neyts, B. Kuyken, D. Van Thourhout, J. Beeckman, Nanophotonic pockels modulators on a silicon nitride platform, Nat. Commun. 9 (2018) 3444.
[4] G. Velarde, S. Pandya, J. Karthik, D. Pesquera, L.W. Martin, Pyroelectric thin films—past, present, and future, APL Mater. 9 (2021) 010702.
[5] Q. Zhang, R.W. Whatmore, Improved ferroelectric and pyroelectric properties in Mn-doped lead zirconate titanate thin films, J. Appl. Phys. 94 (2003) 5228–5233.
[6] A. Sambri, D. Isarakorn, A. Torres-Pardo, S. Gariglio, P. Janphuang, D. Briand, O. Stéphan, J.W. Reiner, J.M. Triscone, N.F. de Rooij, C.H. Ahn, Epitaxial piezoelectric Pb(Zr0.2Ti0.8)O_3thin films on silicon for energy harvesting devices, Smart Mater. Res. 2012 (2012) 426048.
[7] C. Jorel, H. Colder, A. Galdi, L. Méchin, Epitaxial PZT thin films on YSZ-buffered Si (001) substrates for piezoelectric MEMS or NEMS applications, IOP Conf. Ser. Mater. Sci. Eng. 41 (2012) 012012.
[8] T.Q. Shao, T.L. Ren, L.T. Liu, J.U.N. Zhu, Z.J. Li, Fabrication and properties of silicon-based PLZT thin films for MFSFET applications, Integr. Ferroelectr. 61 (2004) 189–195.
[9] C.G. Wu, X.Y. Sun, J. Meng, W.B. Luo, P. Li, Q.X. Peng, Y.S. Luo, Y. Shuai, Fast and wide-band response infrared detector using porous PZT pyroelectric thick film, Infrared Phys. Technol. 63 (2014) 69–73.
[10] C. Huang, D. Li, T. He, Y. Peng, W. Zhou, Z. Yang, J. Xu, Q. Wang, Large quadratic electro-optic effect of the PLZT thin films for optical communication integrated devices, ACS Photonics 7 (2020) 3166–3176.
[11] G.T. Reed, G. Mashanovich, F.Y. Gardes, D.J. Thomson, Silicon optical modulators, Nat. Photonics 4 (2010) 518–526.
[12] H. Ryu, S.W. Kim, Emerging pyroelectric nanogenerators to convert thermal energy into electrical energy, Small 17 (2021) 1903469.
[13] P.S. Anderson, S. Guerin, B.E. Hayden, Y. Han, M. Pasha, K.R. Whittle, I.M. Reaney, Optimization of synthesis of the solid solution, Pb(Zr1–xTix)O3 on a single substrate using a high-throughput modified molecular-beam epitaxy technique, J. Mater. Res. 24 (2009) 164–172.
[14] P.S. Anderson, S. Guerin, B.E. Hayden, M.A. Khan, A.J. Bell, Y. Han, M. Pasha, K. R. Whittle, I.M. Reaney, Synthesis of the ferroelectric solid solution, Pb(Zr1−xTix) O3 on a single substrate using a modified molecular beam epitaxy technique, Appl. Phys. Lett. 90 (2007) 202907.
[15] P. Muralt, Recent progress in materials issues for piezoelectric MEMS, J. Am. Ceram. Soc. 91 (2008) 1385–1396.
[16] D. Ban, G. Liu, H. Yu, X. Sun, N. Deng, F. Qiu, High electro-optic coefficient lead zirconate titanate films toward low-power and compact modulators, Opt. Mater. Express 11 (2021) 1733–1741.
[17] K. Sato, M. Ishii, K. Kurihara, M. Kondo, Crystal orientation dependence of the electro-optic effect in epitaxial lanthanum-modified lead zirconate titanate films, Appl. Phys. Lett. 87 (2005) 251927.
[18] C.C. Mardare, E. Joanni, A.I. Mardare, J.R.A. Fernandes, C.P.M.d. Sá, P.B. Tavares, Effects of adhesion layer (Ti or Zr) and Pt deposition temperature on the properties of PZT thin films deposited by RF magnetron sputtering, Appl. Surf. Sci. 243 (2005) 113–124.
[19] C.H. Park, M.S. Won, Y.H. Oh, Y.G. Son, An XPS study and electrical properties of Pb1.1Zr0.53Ti0.47O3/PbO/Si (MFIS) structures according to the substrate temperature of the PbO buffer layer, Appl. Surf. Sci. 252 (2005) 1988–1997.
[20] T.W. Cornelius, C. Mocuta, S. Escoubas, L.R.M. Lima, E.B. Araújo, A.L. Kholkin, O. Thomas, Piezoelectric properties of Pb(1-x)La(x)(Zr(0.52)Ti(0.48))(1-x/4)O(3) thin films studied by in situ X-ray diffraction, Materials (Basel) 13 (2020) 3338.

[21] W.C. Shih, Z.Z. Yen, Y.S. Liang, Preparation of highly C-axis-oriented PZT films on Si substrate with MgO buffer layer by the sol–gel method, J. Phys. Chem. Solids 69 (2008) 593–596.

[22] D.S. Paik, A.V. Prasada Rao, S. Komarneni, Sol-gel fabrication of oriented PZT thin films: effect of buffer layer in promoting epitaxial growth, Ferroelectrics 211 (1998) 141–151.

[23] J. He, F. Li, X. Chen, S. Qian, W. Geng, K. Bi, J. Mu, X. Hou, X. Chou, Thickness dependence of ferroelectric and optical properties in Pb(Zr0.53Ti0.47)O3 thin films, Sensors 19 (2019) 4073.

[24] Y. Otani, N. Abe, S. Okamura, T. Shiosaki, Influence of post-annealing on the characteristics of Pb(Zr,Ti)O3 thin films deposited by liquid delivery MOCVD using a cocktail solution, Integr. Ferroelectr. 59 (2003) 1475–1482.

[25] C.L. Dai, F.Y. Xiao, C.Y. Lee, Y.C. Cheng, P.Z. Chang, S.H. Chang, Thermal effects in PZT: diffusion of titanium and recrystallization of platinum, Mater. Sci. Eng. A 384 (2004) 57–63.

[26] R. Reshmi, V. Natarajan, M.K. Jayaraj, Effect of buffer layer on the properties of laser ablated PZT thin films, Integr. Ferroelectr. 117 (2010) 104–109.

[27] T. Schneider, D. Leduc, J. Cardin, C. Lupi, N. Barreau, H. Gundel, Optical properties of PZT thin films deposited on a ZnO buffer layer, Opt Mater (Amst) 29 (2007) 1871–1877.

[28] H. Li, S. Wang, J. Jian, H. Dong, J. Chen, D. Jin, J. Cheng, Improved ferroelectric properties of (100)-oriented PZT thin films deposited on stainless steel substrates with La0.5Sr0.5CoO_3 buffer layers, J. Mater. Sci. Mater. Electron. 29 (2018) 14651–14656.

[29] M. Xiao, Z. Zhang, W. Zhang, P. Zhang, Effect of La and W dopants on dielectric and ferroelectric properties of PZT thin films prepared by sol–gel process, Appl. Phys. A 124 (2017) 8.

[30] E. Tokumitsu, K. Itani, B.K. Moon, H. Ishiwara, Preparation of PbZr x Ti 1−x O_3 films on si substrates using $SrTiO_3$ buffer layers, MRS Proc. 361 (1994) 427.

[31] Y. Jeon, D.G. Kim, K. No, S.J. Kim, J.S. Chung, Residual stress analysis of pt bottom electrodes on ZrO_2/SiO_2/Si and SiO_2/Si Substrates for Pb(ZrTi)O_3Thick Films, Jpn. J. Appl. Phys. 39 (2000) 2705–2709.

[32] N.A. Basit, H.K. Kim, J. Blachere, Growth of highly oriented Pb(Zr, Ti)O_3 films on MgO-buffered oxidized Si substrates and its application to ferroelectric nonvolatile memory field-effect transistors, Appl. Phys. Lett. 73 (1998) 3941–3943.

[33] B.T. Liu, C.S. Cheng, F. Li, L. Ma, Q.X. Zhao, Z. Yan, D.Q. Wu, C.R. Li, Y. Wang, X. H. Li, X.Y. Zhang, Ni–Al diffusion barrier layer for integrating ferroelectric capacitors on Si, Appl. Phys. Lett. 88 (2006) 252903.

[34] J.P. George, P.F. Smet, J. Botterman, V. Bliznuk, W. Woestenborghs, D. van Thourhout, K. Neyts, J. Beeckman, Lanthanide-Assisted deposition of strongly electro-optic PZT thin films on silicon: toward integrated active nanophotonic devices, ACS Appl. Mater. Interfaces 7 (24) (2015) 13350–13359.

[35] S. Abel, F. Eltes, J.E. Ortmann, A. Messner, P. Castera, T. Wagner, D. Urbonas, A. Rosa, A.M. Gutierrez, D. Tulli, P. Ma, B. Baeuerle, A. Josten, W. Heni, D. Caimi, L. Czornomaz, A.A. Demkov, J. Leuthold, P. Sanchis, J. Fompeyrine, Large Pockels effect in micro- and nanostructured barium titanate integrated on silicon, Nat. Mater. 18 (2019) 42–47.

[36] S. Abel, J. Fompeyrine, Electro-Optically Active Oxides on Silicon for Photonics, in: Thin Films on Silicon, pp. 455–501.

[37] M. Prabu, I.B. Banu, G.V. Vijayaraghavan, S. Gobalakrishnan, M. Chavali, Pulsed laser deposition and ferroelectric characterization of nanostructured perovskite lead zirconate titanate (52/48) thin films, J. Nanosci. Nanotechnol. 13 (2013) 1938–1942.

[38] I. Kanno, H. Kotera, K. Wasa, T. Matsunaga, T. Kamada, R. Takayama, Crystallographic characterization of epitaxial Pb(Zr,Ti)O3 films with different Zr/Ti ratio grown by radio-frequency-magnetron sputtering, J. Appl. Phys. 93 (2003) 4091–4096.

[39] S. Guerin, B.E. Hayden, Physical vapor deposition method for the high-throughput synthesis of solid-state material libraries, J. Comb. Chem. 8 (2006) 66–73.

[40] S. Guerin, B.E. Hayden, ABO3 and A1−xCxB1−yDy(O1−zEz)3: review of experimental optimisation of thin film perovskites by high-throughput evaporative physical vapour deposition, Chem. Commun. 55 (2019) 10047–10055.

[41] K. Bradley, K. Giagloglou, B.E. Hayden, H. Jungius, C. Vian, Reversible perovskite electrocatalysts for oxygen reduction/oxygen evolution, Chem. Sci. 10 (2019) 4609–4617.

[42] I. Bakaimi, X. He, S. Guerin, N.Z.I. Hashim, Q. Luo, I.M. Reaney, S. Gao, B. E. Hayden, C.H.K. de Groot, Combinatorial synthesis and screening of (Ba,Sr)(Ti, Mn)O3 thin films for optimization of tunable co-planar waveguides, J. Mater. Chem. C 6 (2018) 6222–6228.

[43] R. Bruchhaus, D. Pitzer, M. Schreiter, W. Wersing, Optimized PZT thin films for pyroelectric IR detector arrays, J. Electroceram. 3 (1999) 151–162.

[44] E. Fujii, R. Takayama, K. Nomura, A. Murata, T. Hirasawa, A. Tomozawa, S. Fujii, T. Kamada, H. Torii, Preparation of (001)-oriented Pb(Zr,Ti)O/sub 3/thin films and their piezoelectric applications, IEEE Trans. Ultrason. Ferroelectr. Freq. Control 54 (2007) 2431.

[45] I. Bretos, R. Jiménez, M. Tomczyk, E. Rodríguez-Castellón, P.M. Vilarinho, M. L. Calzada, Active layers of high-performance lead zirconate titanate at temperatures compatible with silicon nano- and microeletronic [corrected] devices, Sci. Rep. 6 (2016) 20143.

[46] N. Ledermann, P. Muralt, J. Baborowski, S. Gentil, K. Mukati, M. Cantoni, A. Seifert, N. Setter, {1 0 0}-Textured, piezoelectric Pb(Zrx, Ti1−x)O_3 thin films for MEMS: integration, deposition and properties, Sens. Actuators A 105 (2003) 162–170.

[47] F. Dauchy, R.A. Dorey, Patterned crack-free PZT thick films for micro-electromechanical system applications, Int. J. Adv. Manuf. Technol. 33 (2007) 86–94.

[48] R. Frunza, D. Ricinschi, F. Gheorghiu, R. Apetrei, D. Luca, L. Mitoseriu, M. Okuyama, Preparation and characterisation of PZT films by RF-magnetron sputtering, J. Alloys Compd. 509 (2011) 6242–6246.

[49] A. Shoghi, A. Shakeri, H. Abdizadeh, M.R. Golobostanfard, Synthesis of crack-free PZT thin films by sol-gel processing on glass substrate, Procedia Mater. Sci. 11 (2015) 386–390.

[50] A.B. Posadas, V.E. Stenger, J. DeFouw, G.Z. Mashanovich, D. Wasserman, A. A. Demkov, Electro-Optic barium titanate modulators on silicon photonics platform, in: Proceedings of the 2023 IEEE Silicon Photonics Conference (SiPhotonics), 2023, pp. 1–2.

[51] P.D. Thacher, Refractive index and surface layers of ceramic (Pb,La)(Zr,Ti)O_3 compounds, Appl. Opt. 16 (1977) 3210–3213.

[52] S. Yang, D. Mo, X. Tang, Spectroscopic ellipsometry studies of amorphous PZT thin films with various Zr/Ti stoichiometries, J. Mater. Sci. 37 (2002) 3841–3845.

[53] A. Deineka, M.D. Glinchuk, L. Jastrabik, G. Suchaneck, G. Gerlach, Ellipsometry investigation of perovskite/pyrochlore PZT thin film stacks, Ferroelectrics 258 (2001) 271–276.

[54] C.J. Kirkby, Dispersion of optical and electro-optic properties of hot-pressed PLZT ceramic materials, Ferroelectrics 7 (1974) 157–159.

[55] C. Millon, C. Malhaire, D. Barbier, Ti and TiOx seeding influence on the orientation and ferroelectric properties of sputtered PZT thin films, Sens. Actuators A 113 (2004) 376–381.

[56] W. Gong, J.F. Li, X. Chu, Z. Gui, L. Li, Combined effect of preferential orientation and Zr/Ti atomic ratio on electrical properties of Pb(ZrxTi1−x)O3 thin films, J. Appl. Phys. 96 (2004) 590–595.

[57] G. Burns, B.A. Scott, Raman spectra of polycrystalline solids; application to the $PbTi_{1-x}Zr_xO_3$ system, Phys. Rev. Lett. 25 (1970) 1191–1194.

[58] G. Burns, B.A. Scott, Lattice modes in ferroelectric perovskites: $pbTiO_3$, Phys. Rev. B 7 (1973) 3088–3101.

[59] P. Ferrari, E. Ramos-Moore, M.A. Guitar, A.L. Cabrera, Raman analysis of ferroelectric switching in niobium-doped lead zirconate titanate thin films, Thin. Solid. Films 556 (2014) 539–543.

[60] J. Frantti, V. Lantto, Structural studies of Nd-modified lead zirconate titanate ceramics between 11 and 680K at the morphotropic phase boundary, Phys. Rev. B 56 (1997) 221–236.

[61] M. Nakajima, H. Nakaki, Y. Ehara, T. Yamada, K. Nishida, T. Yamamoto, M. Osada, H. Funakubo, In situ Raman spectroscopy for characterization of the domain contributions to electrical and piezoelectric responses in Pb(Zr,Ti)O_3 films, Appl. Phys. Lett. 97 (2010) 181907.

[62] S.K. Pandey, A.R. James, R. Raman, S.N. Chatterjee, A. Goyal, C. Prakash, T. C. Goel, Structural, ferroelectric and optical properties of PZT thin films, Physica B 369 (2005) 135–142.

[63] K. Nishida, G. Matuoka, M. Osada, M. Kakihana, T. Katoda, Effects of the substrate on properties of PTO thin film, Appl. Surf. Sci. 216 (2003) 318–322.

[64] H.X. Qin, J.S. Zhu, Z.Q. Jin, Y. Wang, PZT thin films with preferred-orientation induced by external stress, Thin. Solid. Films 379 (2000) 72–75.

[65] X.P. Hu, D.W. Duan, K. Zhang, Y.C. Zhang, S.Q. Chu, J. Zhang, Y.N. Xie, D. Guo, J. L. Cao, Influences of the amorphous phase on local structures and properties of ferroelectric thin films, Ferroelectrics 453 (2013) 149–155.